J Mater Sci

Chemical routes to materials

Improved SERS activity of TiN microstructures by surface modification with Au

Aleksandra Michałowska[1], Aleksandra Szymańska[1,2], Robert Ambroziak[3], Libor Nozka[5], Lukas Vaclavek[4,5], Jan Tomastik[4,5], Sylwia Turczyniak-Surdacka[1], and Jan Krajczewski[1,*]

[1] *Faculty of Chemistry, University of Warsaw, 1 Pasteur St, 02-093 Warsaw, Poland*
[2] *Faculty of Physics, University of Warsaw, 5 Pasteur St, 02-093 Warsaw, Poland*
[3] *Institute of Physical Chemistry, Polish Academy of Sciences, Kasprzaka 44/52, 01-224 Warsaw, Poland*
[4] *Institute of Physics of the Czech Academy of Sciences, Joint Laboratory of Optics of Palacky University, Institute of Physics AS CR, Palacký University Olomouc, 17. Listopadu 50a, 772 07 Olomouc, Czech Republic*
[5] *Joint Laboratory of Optics of Palacký University, Institute of Physics AS CR, Palacký University Olomouc, 17 Listopadu 12, 771 46 Olomouc, Czech Republic*

Received: 24 April 2024
Accepted: 14 August 2024

ABSTRACT

Over the years, numerous outstanding research groups around the world have been working tirelessly on metallic SERS substrates. Although these efforts have led to the development of various sensors and pushed the field forward, today this line of research seems saturated and exhausted. In this work, we address this issue by exploring an emerging topic in recent literature: the fabrication of high-performance TiN SERS-active structures. TiN thin film was sputtered onto pyramidal Si microstructures. Spectroscopic ellipsometry measurements confirmed the plasmonic properties of the TiN material above its plasma wavelength of 515 nm. The Si-TiN surface was subsequently modified with an Au layer, which was then transformed into Au nanoparticles (Au NPs) during the Rapid Thermal Annealing process. The Si-TiN-AuNPs samples exhibited the highest extinction intensity, as well as the best SERS signal intensity for the model Raman reporter molecule. Further analysis of the SERS data showed that the presence of the Au thin film only moderately increased SERS activity, while Au NPs enhanced the SERS signal by one order of magnitude. Final Si-TiN-AuNPs platforms were successfully employed for the detection of vitamin B_{12}, demonstrating a low limit of detection ($8.57 \bullet 10^{-8}$ M) along with excellent point-to-point repeatability.

Handling Editor Maude Jimenez.

Address correspondence to E-mail: jkrajczewski@chem.uw.edu.pl

https://doi.org/10.1007/s10853-024-10120-w
Published online: 13 September 2024

Springer

GRAPHICAL ABSTRACT

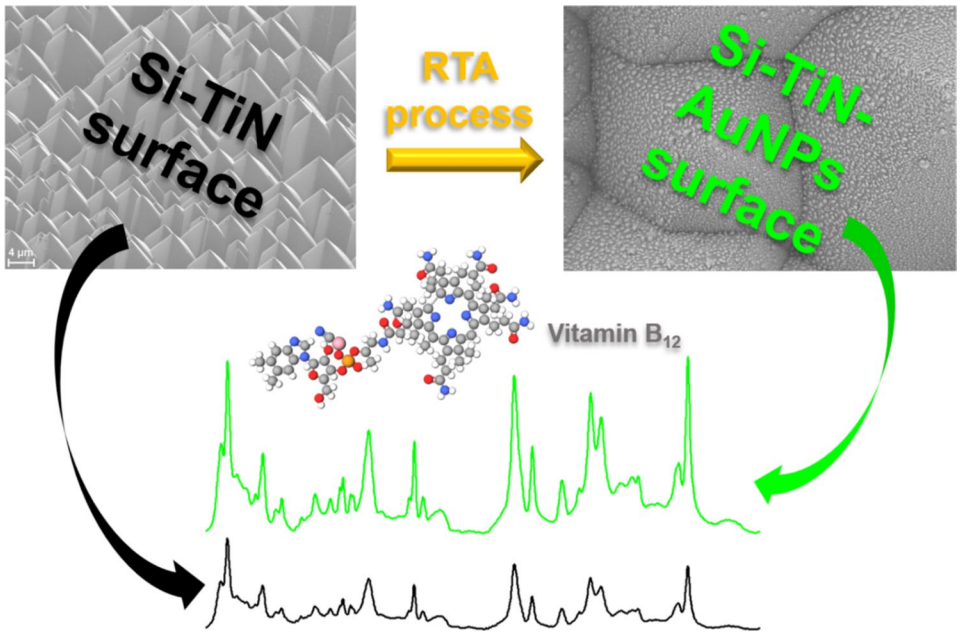

Introduction

Surface-enhanced Raman scattering (SERS) spectroscopy is one of the most sensitive and precise spectroscopic methods suitable for detecting trace amounts of a wide variety of chemical substances[1], [2]. Its outstanding sensitivity arises from the utilization of SERS-active substrates which are usually made out of plasmonic metal and contain some kind of nanofeatures. SERS enhancement is attributed to two independent mechanisms: electromagnetic[3] and/or chemical[4] (also known as charge transfer, CT). The first one comes from the excitation of surface plasmon resonance (SPR) in plasmonic nanostructure which induces a strongly focused electromagnetic (EM) field, leading to a remarkable enhancement of the Raman signal by several orders of magnitude. The chemical enhancement mechanism is related to the charge transfer between substrate material and the analyte molecule. The overall level of enhancement is expressed by the enhancement factor (EF) and its value is determined mostly by the quality of the SERS substrate used[5]. Consequently, SERS performance is intricately linked to the quality of the plasmonic substrate.

The EF is the ratio of the intensity of the SERS signal to the intensity of the non-enhanced Raman signal measured for the same concentration of a given analyte. Some recent papers report values of EF as high as 10^{11} [6] but usually anything above 10^5—10^6 is considered decent[6], [7]. Since EF is inversely proportional to the limit of detection (LOD), it allows for a fair comparison of quality between SERS platforms of different materials. A good quality SERS platform should provide a stable EF over the entire substrate (point-to-point uniformity) and from one substrate to another (sample-to-sample reproducibility), as well as exhibit high chemical and time stability[8], [9]. Therefore, successful and reliable SERS analysis demands meeting numerous requirements imposed on plasmonic nanostructures.

So far, the literature has been dominated by SERS platforms based on plasmonic metals (such as gold [10], silver [11], copper [12], among others) and their bimetallic[13] or trimetallic[14] alloys. In particular, the application of noble metal nanoparticles in SERS spectroscopy has been studied in depth for over 40 years. These efforts allowed for the construction of many sensors, i.e., for detecting DNA mutations, heavy metals, proteins, and various organic compounds like antibiotics, drugs, or pesticides[15–19].

However, due to a very large number of outstanding research groups working tirelessly on metallic SERS substrates all around the world, this line of research seems saturated and exhausted. Moreover, due to the steadily rising prices of Au, which is one of the most popular plasmonic metals for SERS applications, the production cost of gold-based SERS platforms is at an all-time high. What is more, their usability in many kinds of biological or biomedical applications is limited because direct contact of DNA or certain protein strands with bare metals leads to the denaturation of the target molecule. Therefore, there is a great need to search for alternative materials for plasmonic SERS substrates.

Nowadays, TiN nanostructured materials are considered promising as an alternative for noble metals in SERS substrates fabrication[20], [21]. The main research field for nanostructured TiN materials is photocatalysis in heterogeneous catalysis in many chemical reactions, like hydrogen evolution[22], [23] or CO_2 photoreduction[24]. However, some reports confirmed the SERS activity of TiN-based materials[25–28]. So far, the TiN materials are only formed by physical methods like magnetron sputtering[29], [30] or pulsed laser deposition (PLD)[31], [32]. Last year in our research group, we compared TiN and Au SERS platforms with the same morphology[33]. Optical characterization based on diffuse reflectance spectroscopy (DRS) and ellipsometric spectroscopy revealed similar properties of both materials. The SERS spectra analysis has shown that the SERS activity of Au and TiN samples (of the same deposited thickness) is resembling, e.g. they share the same LOD value. That experiment has already proven that TiN can have similar performance to Au while being cheaper and/or more biocompatible. In this work, we show that combining TiN and Au into one nanostructure can result in better performance than with bare TiN or bare Au.

Experimental section

Materials

Si (100) *p*-type wafer, potassium hydroxide, and hydrofluoric acid were acquired from Sigma-Aldrich. Ethanol, acetone, and isopropanol were purchased from Chempur, Piekary Slaskie. The water was purified using a Millipore Milli-Q system (Merck Millipore, Burlington, MA, USA).

Preparation of Si pyramids

To fabricate structures in the shape of pyramids, the chemical wet etching method was employed. Initially, *p*-type silicon wafer Si(100) was cleaved into 1 cm^2 pieces and cleaned using an ultrasound bath containing a solution of ethanol, acetone, and water for approximately 5 min. Then, the Si wafers were immersed in 30% KOH solution at a temperature of 75 °C for 4 min. Subsequently, the wafers were transferred to a solution containing 15% KOH and 5% isopropanol with the temperature gradually increased by 5 °C. After 40 min of such etching, the resulting Si pyramids were rinsed thoroughly with ethanol and water. Finally, to remove any metallic impurities, the silicon pyramids were immersed in a 4% HF solution for 5 min.

Deposition of a TiN layer

Crystalline TiN films were deposited onto the Si pyramids by means of a magnetron sputtering machine operating in a pulsed DC regime. A 4″ titanium target was sputtered in a gas mixture of Ar (99.999%) and N_2 (99,996%). The base pressure before the deposition was typically $1 \bullet 10^{-4}$ Pa. The nitrogen-to-argon flow ratio was 4:15, and a total pressure of 0.2 Pa. A DC power of 700 W (with a power density of 8.6 W/cm^2) was applied in pulsed mode at a frequency of 50 kHz and a duty cycle of 50%. The 80 nm TiN thin film was deposited over a period of 310 s. The target to-substrate distance was maintained at 170 mm.

Deposition of a thin Au film

The deposition of an Au layer onto the Si pyramid substrates was carried out using a Quorum Q150ES sputter coater. A constant current of 20 mA was applied, and the duration of the process was 15 s.

RTA process

The Rapid Thermal Annealing (RTA) process was conducted in an over preheated to 400 °C under ambient air conditions. The sample was rapidly introduced into the oven chamber, and after 30 min it was rapidly removed to return to room temperature.

Experimental techniques

Scanning electron microscopy (SEM) analyses of the SERS-active samples were carried out using a Merlin field emission scanning electron microscope (Zeiss, Germany).

Optical response was analyzed by variable angle spectroscopic ellipsometry (VASE) using a J.A.Woollam M2000-D ellipsometer operating in the wavelength range from 190 to 1000 nm. The angle of incidence was changed from 55° to 75° with a step of 5°. Diffuse reflectance spectra (DRS) were recorded using a Shimadzu UV-2600i spectrometer equipped with an integrating sphere with internal detectors operating in the 1000—200 nm range.

A Microlab 350 spectrometer (Thermo Electron, East Grinstead, UK) was used for the XPS measurements. Al Kα (hν = 1486.6 eV, 300 W) served as the radiation source. Signals were recorded with a hemispherical analyzer at constant pass energies of 100 eV (survey spectra) and 40 eV (high-resolution spectra). The background was corrected using the Shirley model. A mixed asymmetric Gauss/Lorentz function with constant G/L = 0.3 was used to deconvolute the spectra. The band positions were corrected relative to the position of the C1s carbon band at 284.5 eV. An Avantage Surface Chemical Analysis software was used to analyze and develop the results.

Raman spectra were measured using a Horiba Jobin–Yvon Labram HR800 spectrometer coupled with an Olympus BX40 confocal microscope with a long-distance 50 × objective. The Raman spectrometer was equipped with a Peltier-cooled CCD detector (1024 × 256 pixels) and a 600 groove per mm holographic grating, while a He–Ne laser provided the excitation radiation at a wavelength of 633 nm.

Theoretical calculations

For spectral simulations Finite-Difference Time-Domain (FDTD) calculations were performed using Ansys Lumerical FDTD 3D software. Simplified 3D models of the experimental samples were used in all simulations: (1) a 60 nm thick flat TiN layer, (2) an array of Au NPs and (3) an array of Au NPs on a 60 nm thick flat TiN layer; all of them on a flat Si substrate. The TiN and Au materials were represented by dielectric functions of the flat films (deposited in the same manner as in the experiment) obtained by spectroscopic ellipsometry. Si was modeled based on data from the CRC Handbook of Chemistry Physics included in the Lumerical database.

Spectral simulations were performed using a plane wave source (450–980 nm) illuminating the structure from above, perpendicular to the surface. Each simulation region was divided into cubic mesh cells with a maximum size of 1 nm. Periodic conditions with periods from 60 to 200 nm were imposed on the simulation area to account for interparticle interactions. Following the experimental protocol, reflection spectra were calculated in the simulation and then converted to extinction using the Kubelka–Munk function, expressed as $\mathrm{Ext} = \frac{(1-R)^2}{2R}$. Finally, the extinction curves that were obtained were normalized to the intensity of the experimental data for easier comparison.

The electromagnetic field distribution around the Au dimer of nanospheres with a diameter of 70 nm placed on Si and TiN substrate was simulated using the boundary element method (BEM) implemented in the MNPBEM toolbox [34], developed in Matlab®. This toolbox is specifically designed for simulating metallic nanoparticles with BEM.

Results and discussion

Structural properties

In general, anisotropic wet etching involves immersing a substrate in a chemical solution, where the etching rate depends on the crystallographic orientation of the substrate. It is well known from the literature that Si wafers can be etched in an alkaline medium, such as KOH or NaOH solution, leading to the formation of regular shapes, with pyramids being the most common example[35–37]. However, it has been reported that Si wafers with orientation < 100 > give the most repetitive and regular structures, whereas orientations < 110 > and < 111 > do not yield good morphology under the same conditions due to their lower etching rates[23].

SEM was used to structurally characterize the Si pyramids formed. Regular arrays of Si pyramids with an average size of 3.5 ± 0.3 μm were relatively uniformly distributed on the bare Si wafer. SEM images confirmed that the deposited TiN layer is continuous and did not change the morphology of the resulting Si pyramid structures, even after the deposition of a thin Au film.

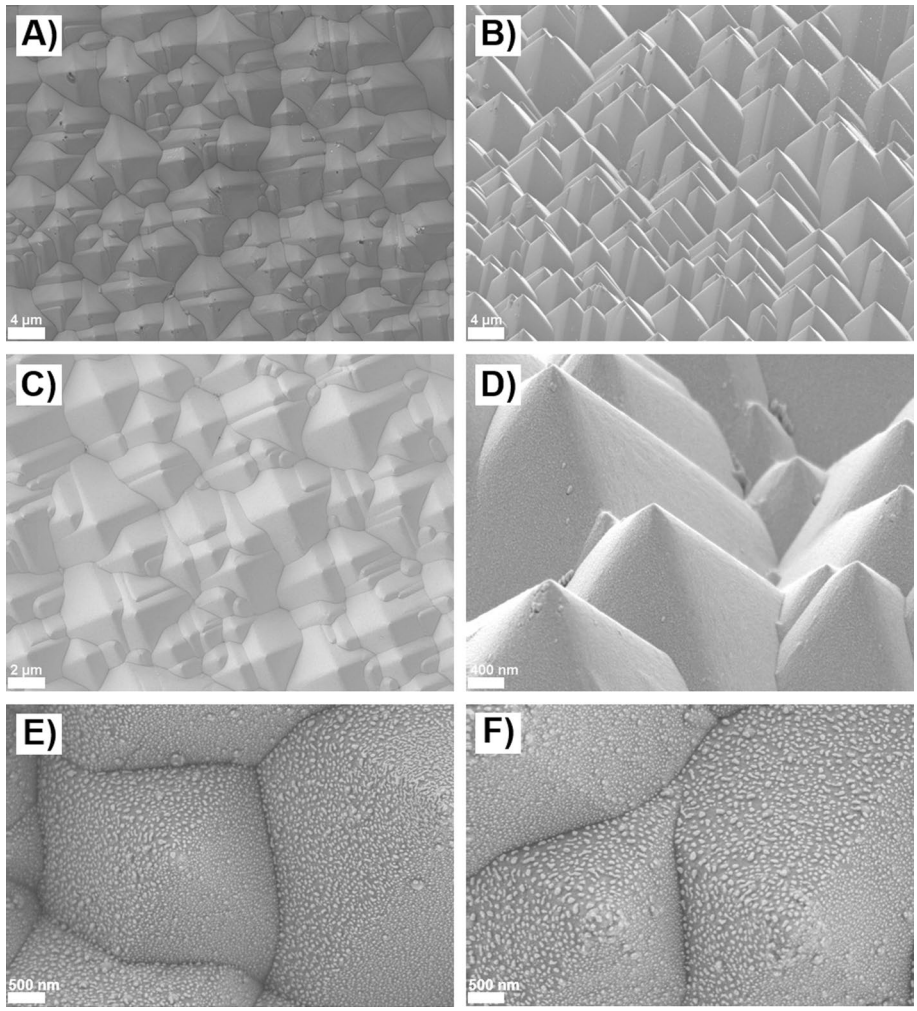

Figure 1 SEM micrographs of Si pyramids coated with: **A**, **B** – 80 nm thick TiN layer; **C**, **D** – 80 nm thick TiN layer and 5 nm thick Au layer; **E**, **F** – 80 nm thick TiN layer and 5 nm thick Au layer which were then annealed at 400°C for 30 min, what led to the formation of Au NPs.

The prepared Si-TiN-Au samples underwent the RTA process. For this purpose, the samples were introduced into a preheated 400 °C oven for 15 min, and then rapidly removed and cooled down to room temperature. It is well known that such processing of Au and Ag thin films (with thickness in the range of 10 nm) can cause cracking of the continuous metal film and lead to the formation of NPs. In our case, SEM images reveal the formation of Au NPs homogeneously distributed on Si-TiN pyramids The entire SEM-based structural characterization is presented in Fig. 1.

Surface elemental composition study (XPS)

As mentioned above, SEM images confirmed that the deposited TiN layer is continuous and does not change the initial morphology of the Si pyramids. XPS measurements were performed to determine the composition of the deposited layer as titanium nitride.

A typical XPS spectrum of TiN exhibits several peaks corresponding to different electronic states of titanium, along with a characteristic peak for nitrogen. The main peaks in the high-resolution TiN spectrum correspond to the $2p_{3/2}$ and $2p_{1/2}$ binding energies, located at 458.3 eV and 463.8 eV, respectively[38]. In addition, low-intensity, broad peaks were observed at higher binding energies in the range of 474 eV to 487 eV and 493 eV to 502 eV, which can be attributed to 1st and 2nd bulk and surface plasmons[38]. In the case of nitrogen, only one strong peak was observed at 396.8 eV, attributed to the N-Ti bonding[38].

In Fig. 2c and d, the Au 4f spectra show the doublet Au $4f_{5/2}$ and Au $4f_{7/2}$ with peak positions located at 87.1 eV and 83.4 eV, respectively. The peaks are split

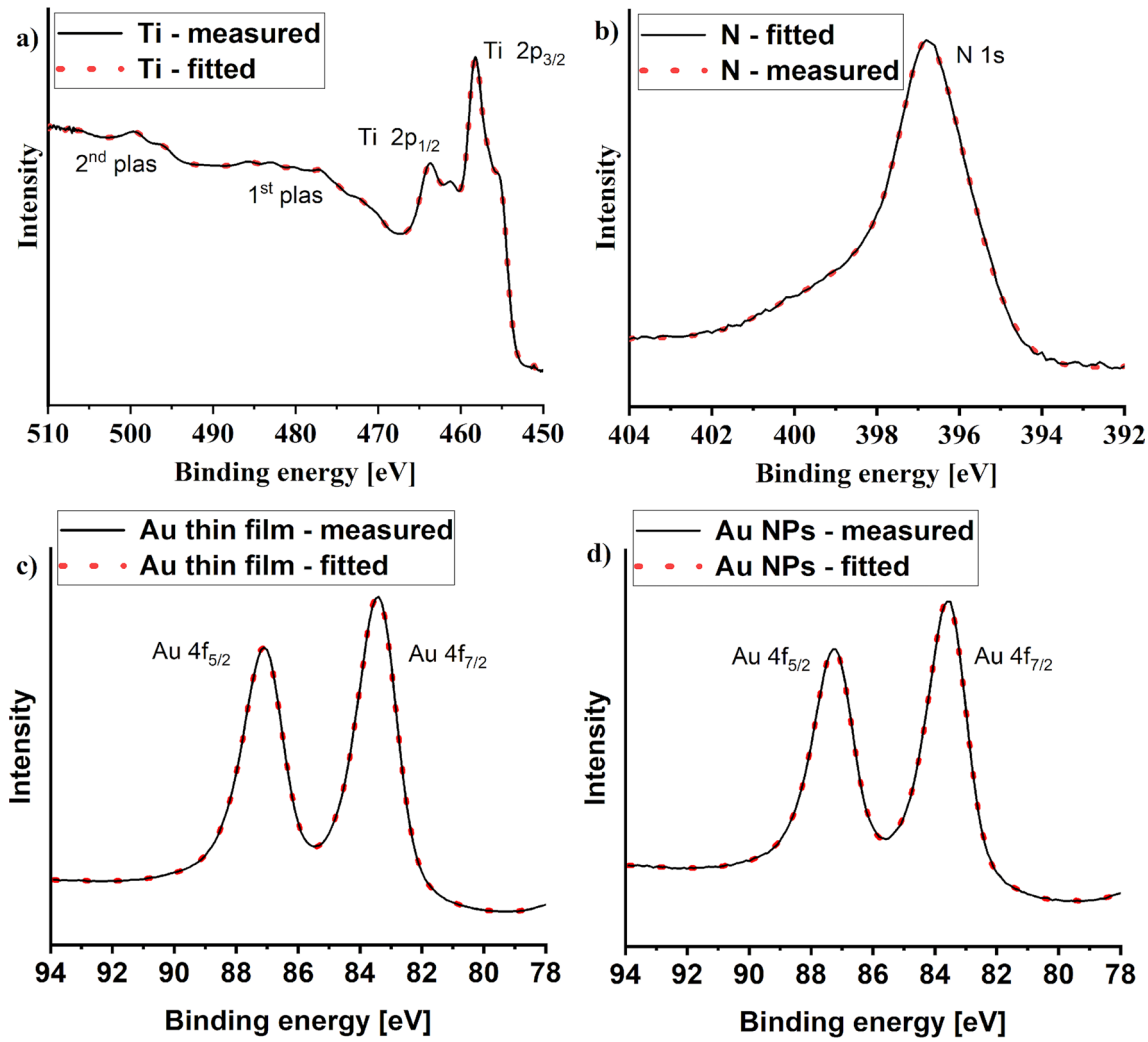

Figure 2 XPS high resolution spectra of **a** Ti, **b** N, **c** Au before and **d** Au after annealing.

by 3.7 eV, indicating the presence of Au in metallic form. It is worth noting that after thermal treatment, the Au peak position shifted by only 0.1 eV, suggesting the same chemical state of Au before and after the RTA process. Based on these results, the observed increase in SERS efficiency of the TiN-Au NPs samples should be attributed to a change in sample morphology rather than any change in Au chemical state or surface concentrations.

Optical properties

Ellipsometry

The optical response of the samples was characterized using VASE measurements and is plotted in Fig. 3 as a pseudo-dielectric function: $\langle\varepsilon\rangle = \langle\varepsilon_1\rangle + i\langle\varepsilon_2\rangle$. The shapes of the curves exhibit typical metallic behavior, with a negative real part $\langle\varepsilon_1\rangle$ for wavelengths higher than the specific plasma wavelength. In this region of wavelengths, electrons effectively screen out the impacting light from the silicon substrate, and the optical response follows the Drude model of metals. Below the plasma wavelength, a dielectric behavior prevails, which can be modeled by a sum of Lorentz oscillators with resonance peaks at specific non-zero frequencies. The plasma wavelength of the Si-TiN sample was identified at 515 nm. According to our assumptions, this wavelength was shifted towards lower values by the additional thin Au layer due to its higher concentration of free electrons. This results in a shift of the plasma wavelength to 495 nm and

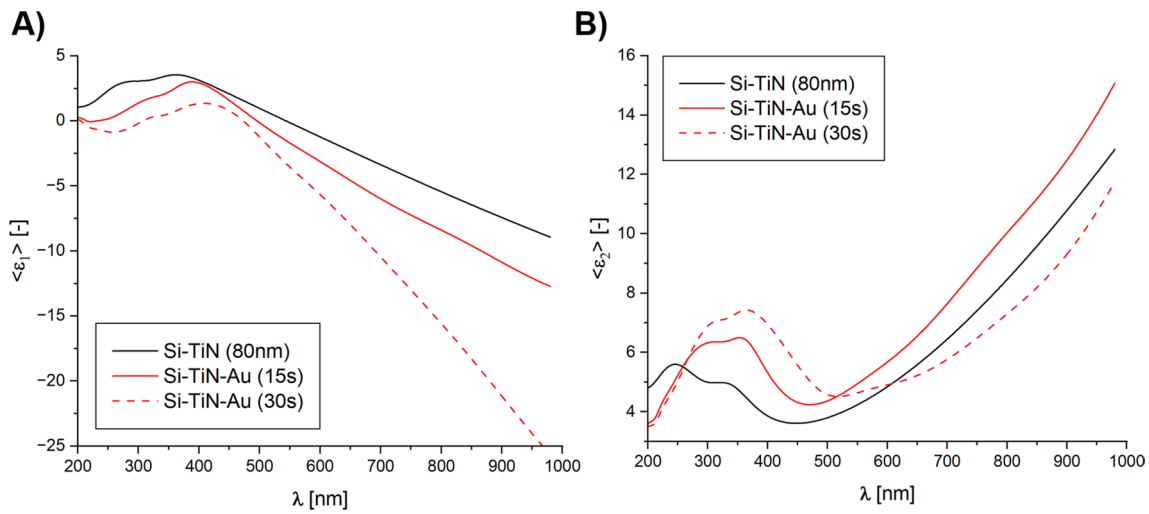

Figure 3 Optical response of samples in the form of the pseudo-dielectric functions: **A** real part, **B** imaginary part.

470 nm for Si-TiN-Au samples annealed for 15 s and 30 s, respectively.

Due to the plasmonic nature of SERS based on the EM enhancement, we were interested in the basic plasmonic characteristics of the samples. More details can be found in here[39], and some results related to these studies are also in here[33]. The very small thickness of the added Au layer results in a mixed response of the TiN-Au system. Based on the values of the pseudo-dielectric function, we calculated "effective" propagation lengths $\langle L_{SPP} \rangle$ of surface-plasmon polaritons (SPPs)[33], [39] assuming water as the ambient medium: 170 nm (Si-TiN), 240 nm (Si-TiN-Au (15 s)), and 375 nm (Si-TiN-Au (30 s)). For a pure Au layer in water, the value of L_{SPP} is around 3.4 μm (calculated using a sample reported in here [33], where the plasmonic analysis was conducted with air as an ambient medium). Thus, the underlying TiN layer mostly defines the value of $\langle L_{SPP} \rangle$. The penetration depth of SPPs into the material was calculated as 17 nm (Si-TiN), 14 nm (Si-TiN-Au (15 s)), and 12 nm (Si-TiN-Au (30 s)). For comparison, the penetration depth of a pure Au layer is 10 nm (again, calculated using a sample reported here[39]). The penetration depth of TiN is higher due to a lower concentration of free electrons with respect to gold. Due to the very small range of the penetration depth compared to the propagation length, the SPP modes are truly trapped EM surface waves.

Diffuse reflectance measurements

The optical properties of the materials have a significant impact on SERS performance. Therefore, the optical response of the formed materials was investigated by UV–Vis spectroscopy. Due to the fact that the samples are not transparent, transmission measurements were excluded, hence DRS measurements were performed. It should be noted that in this type of measurement, it is not possible to distinguish between signals from both absorption and scattering processes. Therefore, the collected data represent extinction (understood as extinction = absorption + scattering).

Figure 4a shows experimentally collected spectra for various materials. The TiN samples exhibit a peak with the maximum located at about 400 nm, which is typical for annealed TiN samples[40]. The spectra of Au-coated samples exhibit low and broad peaks in the range of 500–800 nm. However, after the RTA process, the intensity of such peaks significantly increases. This behavior is typical for both un-annealed and annealed Au films[41]. The higher optical response in region 500–800 nm is attributed to the transformation of Au thin film into Au NPs during the RTA process. It is worth mentioning that the optical behavior of the Au thin film remains the same regardless of the sample composition; the effect observed for Si-TiN pyramids is the same as that for Si pyramids.

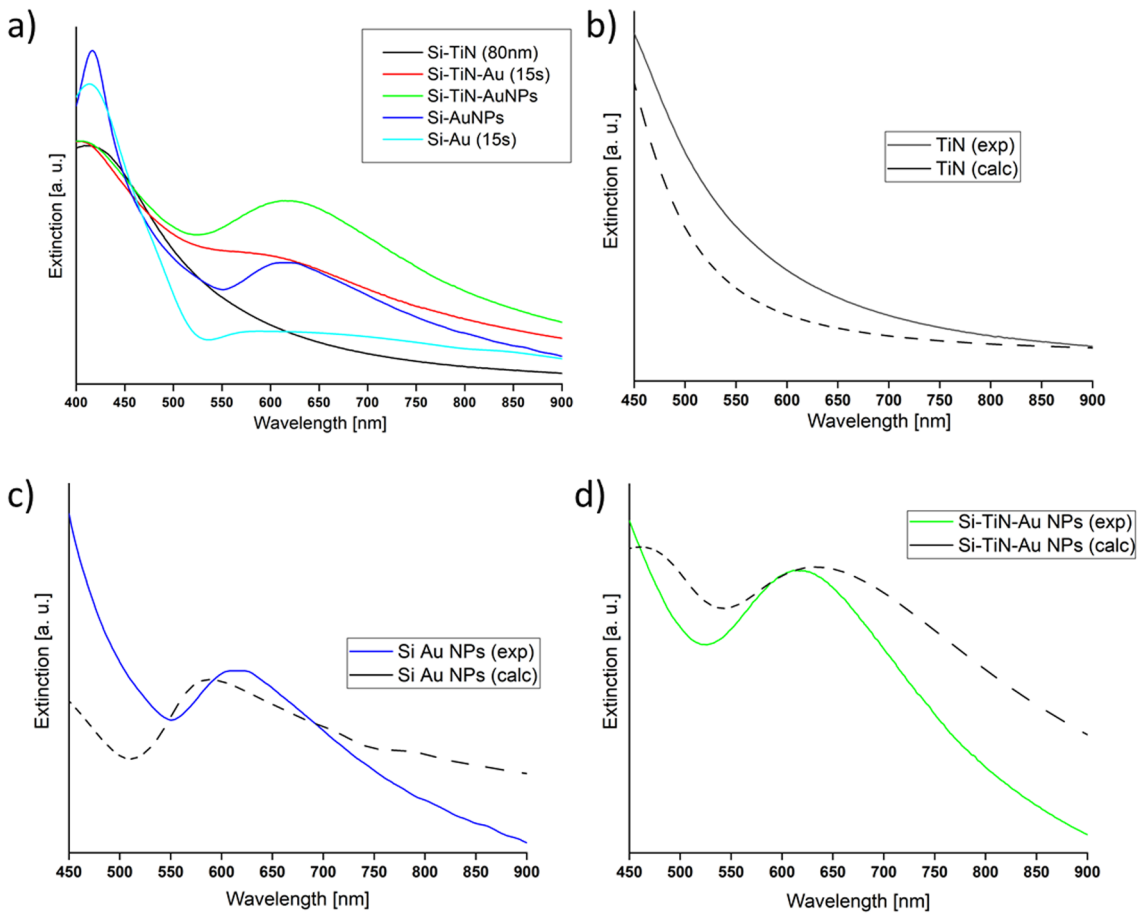

Figure 4 **a** DRS spectra of formed samples; experimental and calculated DRS spectra of **b** TiN, **c** Si Au NPs, **d** Si TiN Au NPs.

FDTD calculations

To estimate the geometrical parameters of the most representative nanostructure, FDTD 3D calculations were performed (see Materials section for details). The simulations did not account for the pyramidal shape of the Si substrate and a simplified model of TiN-Au nanostructure on flat Si was used. First, the optical response of a 60 nm thick TiN film was calculated (Fig. 4b) to confirm the extinction spectra for the new material. Since the experimental and theoretical curves showed great resemblance, it was then proceeded to find the most representative geometry of Au NPs. For this purpose, a series of calculations were performed, including models of Au nanoparticles with different diameters and different simulation region periods (translating to distance between NPs).

Since it is very challenging to reproduce the random distribution of NPs in FDTD calculations, simulations of NPs with a periodic distribution were performed. This allowed us to determine which NP geometry is responsible for most of the plasmonic enhancement. The peaks around ~ 620 nm seen in Fig. 4c and d shifted toward longer wavelengths as the distance between nanoparticles decreased[42], [43]. This behavior is typically observed in the nanogap mode: a resonance that occurs between two objects separated by a distance of several nanometers, in this case, the gap formed between NPs. Regardless of the NPs size, the best resemblance between experimental and calculated curves occurred for nanoparticles 20 nm apart, when the ~ 620 nm peak reaches a proper contrast resembling that seen in the experimental curve. For periods greater than 20 nm, the contrast of this peak is poor and its position is way below 600 nm. As the interparticle distance increases, the peak position is blueshifting and the resonance peak eventually

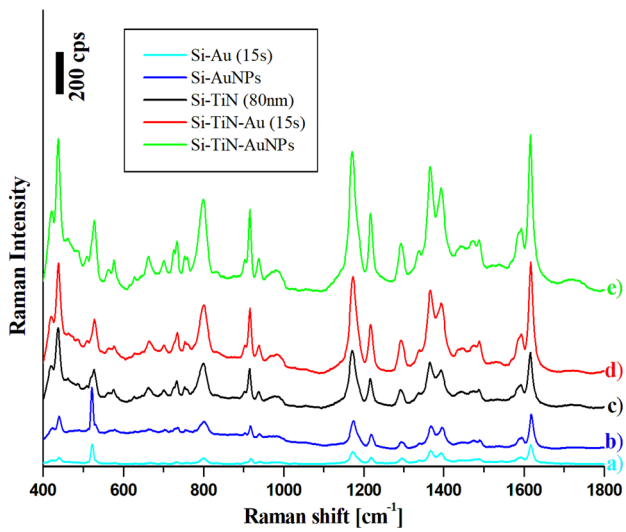

Figure 5 SERS spectra of malachite green in concentration 10^{-5} M recorded on **a** Si-Au (15 s) **b** Si-AuNPs **c** Si-TiN (80 nm) **d** Si-TiN-Au (15 s) and **e** Si-TiN-AuNPs.

disappears (because the NPs are so far away that it is difficult to identify any gap between them).

The best overall similarity between the experimental and calculated curves was obtained for Au NPs with 70 nm in diameter. Thus, Fig. 4c shows the extinction curve calculated for Au NPs with a diameter of 70 nm and a period of 90 nm translating into 20 nm of interparticle distance. Figure 4d refers to the same NPs with a 60 nm TiN layer beneath them. Specifying the diameter as 70 nm allowed the best reproduction of the resonant wavelength. The presence of a nanogap EM field enhancement in the SERS-active substrate is desirable as it usually translates into low LOD values, which are discussed later in this article.

SERS measurements for model analytes

SERS measurements employed a 50 × long-distance objective and a 632.8 nm excitation line. The samples were prepared by applying the volume of 10 μl of dye solution at a concentration of 10^{-5} M onto the samples and then placed in an incubator until the droplet had completely dried. Malachite green (MG) was used as the model molecule to examine the activity of prepared Si-Au, Si-AuNPs, Si-TiN, Si-TiN-Au, and Si-TiN-AuNPs samples for SERS applications. The obtained results were averaged from 50 measurements, as presented in Fig. 5.

MG, a synthetic dye, has found various applications[44], including use as a dye for textiles, leather, and paper. However, its use has raised concerns due to its potential toxicity to humans and the environment[43], [44]. The molecule consists of a tricyclic structure with nitrogen-containing heterocycles, resulting in a rich Raman spectrum. Vibrational modes associated with different parts of MG can be identified and analyzed through Raman spectroscopy. Consistent with prior research, primary peaks associated with the MG molecule were identified at approximately 1175 cm^{-1}, 1217 cm^{-1}, 1396 cm^{-1}, and 1618 cm^{-1}, corresponding to the in-plane vibrations of ring C–H, rocking of C–H, stretching of N-phenyl, and stretching of ring C–C, respectively [45–47]. Other bands observed at frequencies around 916 cm^{-1}, 802 cm^{-1}, and 440 cm^{-1} can be assigned to vibrations related to ring-breathing, out-of-plane phenyl–H bending, and out-of-plane phenyl-C-phenyl bending[47], [48]. These characteristic peaks of MG are clearly observed in the spectra (see Fig. 5). The peak at 520 cm^{-1}, associated with the Si phonon vibration, was also observed. Nevertheless, this peak did not cause interference with the SERS spectra of the employed dye.

In our previous paper[33], we demonstrated that TiN (80 nm) modified Si pyramids exhibit good SERS activity, comparable to those of Au (80 nm) modified Si pyramids. Further modification of TiN thin film deposited on Si pyramids by a 5 nm Au layer resulted in only a moderate increase in SERS activity. However, after the RTA process, during which the Au thin film is converted into semi-spherical Au NPs, the SERS signal increased almost one order of magnitude compared to the Si-TiN sample.

During our research, we also proved that the observed high SERS enhancement of the final Si-TiN-AuNPs sample cannot solely be attributed to the presence of Au material on the surface of the Si pyramids. To investigate this further, we tested samples not only with Si-TiN pyramids covered with Au NPs (green curve in Fig. 5) but also coated with a 5 nm Au thin film (before the RTA process; red curve in Fig. 5). As presented in Fig. 5, samples without NPs exhibit lower SERS enhancement compared to the TiN-Au-NPs samples.

The Si-TiN-AuNPs sample provides the strongest signal among the five samples tested. Generally, at the resonance wavelength of approximately 620 nm (see Fig. 3a), Au provides a better combination of

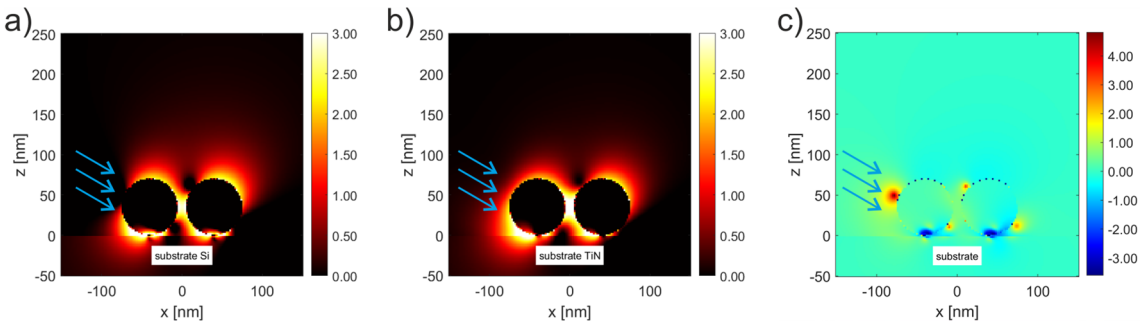

Figure 6 Results of simulations of the field enhancement (in terms of $\log_{10}(\text{Mloc}^2)$) around the Au dimer of nanospheres with a diameter of 70 nm. Dimer was placed on **a)** Si substrate, and **b)** TiN substrate both surrounded by water. The excitation plane-wave had a wavelength of 633 nm and was incident at an angle of 60° relative to the substrate normal, as indicated by the blue arrows. . The lightwave vector, direction, and dimer axis lay in the same xz plane. The ratio of field enhancements between **a)** and **b)** is shown in **c)** in terms of $\log_{10}(\text{Mloc}^2(\text{TiN})/\text{Mloc}^2(\text{Si}))$. Red points indicate response with TiN substrate is higher than the one with Si substrate and blue points indicate the opposite case. Calculations were based on the boundary elements method implemented in the software MNPBEM[34].

permittivity values than TiN: $\text{real}(\varepsilon_{Au}) = -11$ and $\text{im}(\varepsilon_{Au}) = 1.25$, compared to $\text{real}(\varepsilon_{TiN}) = -2.5$ and $\text{im}(\varepsilon_{TiN}) = 5.5$. Nevertheless, TiN exhibits plasmonic properties above 470 nm in this setup (see Sect. "Ellipsometry"), allowing the EM field from TiN to influence the neighboring NP's field, and leading to plasmonic coupling. Thus, instead of the usual blueshift and deterioration of the resonance due to the presence of a material with a lower refractive index ($n_{TiN} = 1.9$ vs $n_{Si} = 3.5$), we observe an increase in the resonance peak amplitude and its broadening (see Fig. 3a). Plasmonic coupling can enhance the local EM field intensity, which is beneficial for SERS. First, higher EM field amplitude generates a stronger SERS signal, translating into higher SERS gain and lower LOD. Second, broadening the resonance can improve the light-matter interaction over a wider frequency range, enhancing both incident and Raman scattered (Stokes) photons, which ultimately contributes to a higher overall SERS signal, as seen in Fig. 5 (compare dark blue and green curves).

It is worth mentioning that the permittivity values suggest the Si-Au sample should provide a higher signal than Si-TiN. However, the thicknesses of the materials are drastically different (80 nm of TiN vs 5 nm of Au) and cannot be directly compared.

These results indicate that in order to improve the stability of noble metal SERS-active substrates, using TiN may be a better choice than any other dielectric materials. Ordinary dielectrics like SiO_2 or Al_2O_3 between the Si substrate and AuNP can stabilize Au but deteriorate the observed SERS signal due to their lower refractive index compared to Si. Similarly, when Au is covered with dielectric, the EM field is trapped at the Au-dielectric interface, a site inaccessible to analyte molecules, negatively affecting the SERS signal. TiN, however, can stabilize and enhance the signal due to the plasmonic coupling. A similar effect was observed with Ag-TiN nanostructures, where the deposition of a thin TiN layer around Ag nanostructures led to an increase in SERS activity[49]. In such cases, the EM field is not trapped between the layers but is located on the outer part of the nanostructures, beneficial for SERS applications.

Additionally, the simulations of the electromagnetic field enhancement around the dimer composed of Au nanospheres with a diameter of 70 nm were conducted, see Fig. 6. In the first case, the dimer was placed on an Si wafer, while in the second case on a TiN substrate. The excitation plane wave had a wavelength of 633 nm, equal to one used in SERS measurements. The direction of light propagation was 60° with respect to the substrate normal, see blue arrows in the figure, which mimicked the tilt of pyramid walls with respect to the sample normal (and the direction of the light propagation during SERS measurements). Raman reporter molecules preferentially stick to the dimer from above as indicated by the same blue arrows in the figure. They experience a higher local field in the case of TiN-Au in this area as indicated in Fig. 6c. Their Raman response is thus amplified more than in the case of the Si-Au system.

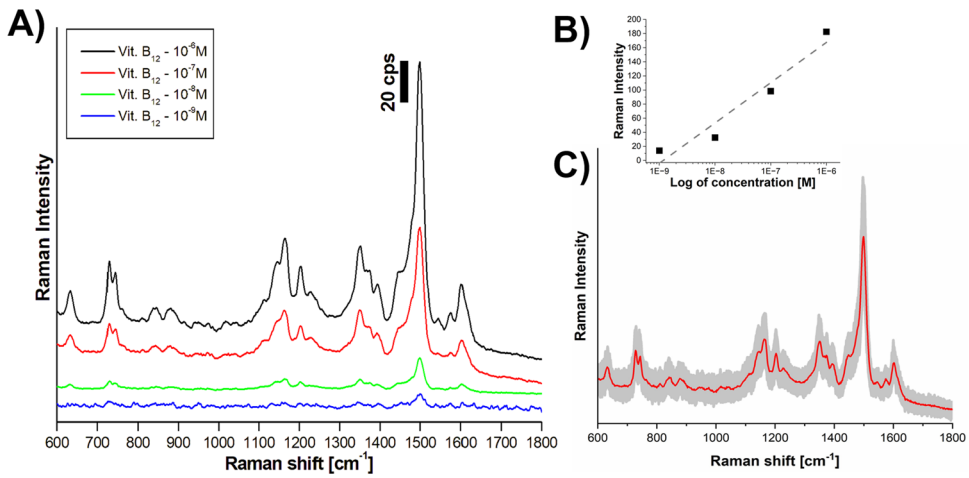

Figure 7 **A)** SERS spectra of vit. B_{12} at various concentrations recorded on Si-TiN-AuNPs sample. **B)** Limit of detection (LOD) determination towards vit. B_{12}. **C)** Point-to-point analysis for Si-TiN-AuNPs sample for vit. B_{12} with 10^{-7}M concentrations.

SERS detection of vitamin B_{12}

The sample exhibiting the highest EF was subjected to vitamin B_{12} detection. Aqueous solutions of vitamin B_{12} with various concentrations (ranging from 10^{-5} M to 10^{-9} M) were prepared, and SERS spectra were recorded, SERS spectra are presented in Fig. 7. Even at concentrations as low as 10^{-9} M, the characteristic peak located at 1498 cm^{-1}, related to corrin ring vibration modes[33], was still observable.

Based on recorded SERS spectra, the Raman intensity of the strongest band (located at 1498 cm^{-1}) was plotted against the logarithm of concentrations. As a result, the LOD was determined to be $8.57 \bullet 10^{-8}$ M. Additionally, the point-to-point analysis revealed good sample homogeneity and low dispersion of recorded SERS spectra.

Conclusion

In this study, we demonstrate the high SERS activity of TiN thin film deposited on pyramidal Si microstructures. By adding an Au thin film to the Si-TiN surface and further modifying it with the RTA treatment, we showed that the SERS signal intensity could be elevated even by one order of magnitude. Structural properties and surface elemental composition were analyzed using SEM and XPS measurements. The optical properties of the prepared materials were investigated via UV–Vis DRS and spectroscopic ellipsometry, confirming the plasmonic properties of TiN thin film on Si microstructures. Additionally, ellipsometric measurements revealed that the plasmonic properties of TiN improved after Au NPs decoration. FDTD simulations confirmed the absorbance spectra obtained in the experiment and identified the most representative nanostructure responsible for the SERS enhancement: a 20 nm gap between AuNPs. The SERS activity was evaluated using the model Raman-reporter molecule malachite green (MG). Data analysis confirmed that the SERS activity of the TiN thin film increased after the deposition of Au in the form of a thin film (moderate enhancement growth) or NPs (one order of magnitude higher enhancement). This behavior is attributed to the plasmonic coupling between TiN and AuNP, which increases the local EM field intensity and broadens the resonance, contributing to an overall improvement in light-matter interaction over a broader frequency range. The most active Si-TiN-AuNPs samples were employed for the detection of vitamin B_{12} with a low LOD of 10^{-9} M and excellent point-to-point repeatability. We strongly believe that TiN-noble metal nanocomposites could pave the way for highly active SERS platforms having excellent properties and stability.

Acknowledgements

J.K. thanks the University of Warsaw, Faculty of Chemistry for its financial support.
L. Nozka gratefully acknowledge the support from the project OP JAC CZ.02.01.01/00/22_008/0004631 (MATUR) of MSMT of the Czech Republic and IGA_PrF_2023_005 of Palacky University in Olomouc.

Funding

Libor Nozka - OP JAC CZ.02.01.01/00/22_008/0004631 (MSMT of the Czech Republic), IGA_Prf_2024_04 (Palacky University in Olomouc).

Data availability

The data that support the findings of this study are available in the Zenodo open database at https://zenodo.org/records/10855219, reference number 10855219. (DOI: https://doi.org/10.5281/zenodo.10855219)

Declarations

Conflicts of interest The authors declare no conflict of interest for the research presented here.

References

[1] Liu H, Zhang L, Lang X, Yamaguchi Y, Iwasaki H, Inouye Y, Xue Q, Chen M (2011) Single molecule detection from a large-scale SERS-active $Au_{79}Ag_{21}$ substrate. Sci Rep 1(1):112. https://doi.org/10.1038/srep00112

[2] Chen H-Y, Lin M-H, Wang C-Y, Chang Y-M, Gwo S (2015) Large-scale hot spot engineering for quantitative SERS at the single-molecule scale. J Am Chem Soc 137(42):13698–13705. https://doi.org/10.1021/jacs.5b09111

[3] Tian Z-Q, Ren B, Wu D-Y (2002) Surface-enhanced Raman scattering: from noble to transition metals and from rough surfaces to ordered nanostructures. J Phys Chem B 106(37):9463–9483. https://doi.org/10.1021/jp0257449

[4] Otto A (1991) Surface-enhanced Raman scattering of adsorbates. J Raman Spectrosc 22(12):743–752. https://doi.org/10.1002/jrs.1250221204

[5] Wang X, Huang S-C, Hu S, Yan S, Ren B (2020) Fundamental understanding and applications of plasmon-enhanced Raman spectroscopy. Nat Rev Phys 2(5):253–271. https://doi.org/10.1038/s42254-020-0171-y

[6] Cai J, Liu R, Jia S, Feng Z, Lin L, Zheng Z, Wu S, Wang Z (2021) SERS hotspots distribution of the highly ordered noble metal arrays on flexible substrates. Opt Mater 122:111779. https://doi.org/10.1016/j.optmat.2021.111779

[7] Zhou H, Qiu J, Zhang Y, Liang Y, Han L, Zhang Y (2024) Self-Assembled C-Ag hybrid nanoparticle on Nanoporous GaN enabled ultra-high enhancement factor SERS sensor for sensitive thiram detection. J Hazard Mater 469:133868. https://doi.org/10.1016/j.jhazmat.2024.133868

[8] Porter MD, Granger JH (2017) Surface-enhanced Raman scattering II: concluding remarks. Faraday Discuss 205:601–613. https://doi.org/10.1039/C7FD00206H

[9] Natan MJ (2006) Concluding remarks : surface enhanced Raman scattering. Faraday Discuss 132:321. https://doi.org/10.1039/b601494c

[10] Kundu S (2013) A new route for the formation of Au nanowires and application of shape-selective Au nanoparticles in SERS studies. J Mater Chem C 1(4):831–842. https://doi.org/10.1039/C2TC00315E

[11] Zhao Y, Zhang Y-J, Meng J-H, Chen S, Panneerselvam R, Li C-Y, Jamali SB, Li X, Yang Z-L, Li J-F, Tian Z-Q (2016) A Facile method for the synthesis of large-size Ag nanoparticles as efficient SERS substrates: large-size Ag nanoparticles as efficient SERS substrates. J Raman Spectrosc 47(6):662–667. https://doi.org/10.1002/jrs.4879

[12] Santos EDB, Sigoli FA, Mazali IO (2013) Metallic Cu nanoparticles dispersed into porous glass: a simple green chemistry approach to prepare SERS substrates. Mater Lett 108:172–175. https://doi.org/10.1016/j.matlet.2013.06.110

[13] Fan M, Lai F-J, Chou H-L, Lu W-T, Hwang B-J, Brolo AG (2013) Surface-enhanced Raman scattering (SERS) from Au: Ag bimetallic nanoparticles: the effect of the molecular probe. Chem Sci 4(1):509–515. https://doi.org/10.1039/C2SC21191B

[14] Chang K, Chung H (2016) Simple electrochemical synthesis of an Au–Ag–Cu trimetallic nanodendrite and its use as

a SERS substrate. RSC Adv 6(79):75943–75950. https://doi.org/10.1039/C6RA01670G

[15] Wu L, Teixeira A, Garrido-Maestu A, Muinelo-Romay L, Lima L, Santos LL, Prado M, Diéguez L (2020) Profiling DNA Mutation patterns by SERS fingerprinting for supervised cancer classification. Biosens Bioelectron 165:112392. https://doi.org/10.1016/j.bios.2020.112392

[16] Chen L, Zhao Y, Wang Y, Zhang Y, Liu Y, Han XX, Zhao B, Yang J (2016) Mercury species induced frequency-shift of molecular orientational transformation based on SERS. Analyst 141(15):4782–4788. https://doi.org/10.1039/C6AN00945J

[17] Li H, Wang M, Shen X, Liu S, Wang Y, Li Y, Wang Q, Che G (2019) Rapid and sensitive detection of enrofloxacin hydrochloride based on surface enhanced Raman scattering-active flexible membrane assemblies of ag nanoparticles. J Environ Manag 249:109387. https://doi.org/10.1016/j.jenvman.2019.109387

[18] Kołątaj K, Krajczewski J, Kudelski A (2018) Dipyramidal-Au@SiO2 nanostructures: new efficient electromagnetic nanoresonators for Raman spectroscopy analysis of surfaces. Appl Surf Sci 456:932–940. https://doi.org/10.1016/j.apsusc.2018.06.208

[19] Wang K, Sun D-W, Pu H, Wei Q (2020) A rapid dual-channel readout approach for sensing carbendazim with 4-aminobenzenethiol-functionalized core-shell Au@Ag nanoparticles. Analyst 145(5):1801–1809. https://doi.org/10.1039/C9AN02185J

[20] Patsalas P, Kalfagiannis N, Kassavetis S (2015) Optical properties and plasmonic performance of titanium nitride. Materials 8(6):3128–3154. https://doi.org/10.3390/ma8063128

[21] Cortie MB, Giddings J, Dowd A (2010) Optical properties and plasmon resonances of titanium nitride nanostructures. Nanotechnology 21(11):115201. https://doi.org/10.1088/0957-4484/21/11/115201

[22] Meng X, Qi W, Kuang W, Adimi S, Guo H, Thomas T, Liu S, Wang Z, Yang M (2020) Chromium-Titanium nitride as an efficient co-catalyst for photocatalytic hydrogen production. J Mater Chem A 8(31):15774–15781. https://doi.org/10.1039/D0TA00488J

[23] Liu S, Qi W, Adimi S, Guo H, Weng B, Attfield JP, Yang M (2021) Titanium nitride-supported platinum with metal-support interaction for boosting photocatalytic H_2 evolution of indium sulfide. ACS Appl Mater Interfaces 13(6):7238–7247. https://doi.org/10.1021/acsami.0c20919

[24] Zhou X, Zolnhofer EM, Nguyen NT, Liu N, Meyer K, Schmuki P (2015) Stable Co-Catalyst-Free photocatalytic H_2 Evolution from oxidized titanium nitride nanopowders. Angew Chem Int Ed 54(45):13385–13389. https://doi.org/10.1002/anie.201506797

[25] Zhao J, Lin J, Wei H, Li X, Zhang W, Zhao G, Bu J, Chen Y (2015) Surface enhanced Raman scattering substrates based on titanium nitride nanorods. Opt Mater 47:219–224. https://doi.org/10.1016/j.optmat.2015.04.067

[26] Wei H, Wu M, Dong Z, Chen Y, Bu J, Lin J, Yu Y, Wei Y, Cui Y, Wang R (2017) Composition, microstructure and SERS Properties of titanium nitride thin film prepared via Nitridation of sol-gel Derived titania thin films. J Raman Spectrosc 48(4):578–585. https://doi.org/10.1002/jrs.5080

[27] Lorite I, Serrano A, Schwartzberg A, Bueno J, Costa-Krämer JL (2013) Surface enhanced Raman spectroscopy by titanium nitride non-continuous thin films. Thin Solid Films 531:144–146. https://doi.org/10.1016/j.tsf.2013.01.024

[28] Esmaeilzadeh M, Dizajghorbani-Aghdam H, Malekfar R (2021) Surface-enhanced Raman scattering of methylene blue on titanium nitride nanoparticles synthesized by laser ablation in organic solvents. Spectrochim Acta Part A Mol Biomol Spectrosc 257:119721. https://doi.org/10.1016/j.saa.2021.119721

[29] Jeyachandran YL, Narayandass Sk, Mangalaraj D, Areva S, Mielczarski JA (2007) Properties of titanium nitride films prepared by direct current magnetron sputtering. Mater Sci Eng: A 445–446:223–236. https://doi.org/10.1016/j.msea.2006.09.021

[30] Merie V, Pustan M, Negrea G, Bîrleanu C (2015) Research on titanium nitride thin films deposited by reactive magnetron sputtering for MEMS applications. Appl Surf Sci 358:525–532. https://doi.org/10.1016/j.apsusc.2015.07.063

[31] Major B, Mróz W, Wierzchoń T, Waldhauser W, Lackner J, Ebner R (2004) Pulsed laser deposition of advanced titanium nitride thin layers. Surf Coat Technol 180–181:580–584. https://doi.org/10.1016/j.surfcoat.2003.10.154

[32] Guo H, Chen W, Shan Y, Wang W, Zhang Z, Jia J (2015) Microstructures and properties of titanium nitride films prepared by pulsed laser deposition at different substrate temperatures. Appl Surf Sci 357:473–478. https://doi.org/10.1016/j.apsusc.2015.09.061

[33] Krajczewski J, Michałowska A, Čtvrtlík R, Nožka L, Tomáštík J, Václavek L, Turczyniak-Surdacka S, Bieńskowski K, Solarska R (2023) The battle for the future of SERS—TiN vs Au thin films with the same morphology. Appl Surf Sci 618:156703. https://doi.org/10.1016/j.apsusc.2023.156703

[34] Hohenester U, Trügler A (2012) MNPBEM—A Matlab toolbox for the simulation of plasmonic nanoparticles. Comput Phys Commun 183(2):370–381. https://doi.org/10.1016/j.cpc.2011.09.009

[35] Mahmoud Al A, Lahlouh B (2017) Silicon pyramid structure as a reflectivity reduction mechanism. J of Appl Sci 17(8):374–383. https://doi.org/10.3923/jas.2017.374.383

[36] Leem JW, Dudem B, Yu JS (2017) Biomimetic nano/micro double-textured silicon with outstanding antireflective and super-hydrophilic surfaces for high optical performance. RSC Adv 7(54):33757–33763. https://doi.org/10.1039/C7RA06444F

[37] Iqbal S, Zhang L-J, Fu X-C, Su D, Zhou H-L, Wu W, Zhang T (2018) Highly-efficient low cost anisotropic wet etching of silicon wafers for solar cells application. AIP Adv 8(2):025223. https://doi.org/10.1063/1.5012125

[38] Jaeger D, Patscheider J (2012) A Complete and self-consistent evaluation of XPS spectra of TiN. J Electron Spectrosc Relat Phenom 185(11):523–534. https://doi.org/10.1016/j.elspec.2012.10.011

[39] Le Ru EC, Etchegoin PG (2009) SERS Enhancement Factors and Related Topics. Principles of Surface-Enhanced Raman Spectroscopy. Elsevier, New Zealand, pp 185–264. https://doi.org/10.1016/B978-0-444-52779-0.00010-6

[40] Kavitha A, Kannan R, Sreedhara Reddy P, Rajashabala S (2016) The effect of annealing on the structural, optical and electrical properties of titanium nitride (TiN) thin films prepared by dc magnetron sputtering with supported discharge. J Mater Sci: Mater Electron 27(10):10427–10434. https://doi.org/10.1007/s10854-016-5130-0

[41] Thien ND, Hoa NQ, Doanh SC, ThCh NT, An DK, Long NN, VanVu L (2022) Effect of Au thin film thickness and surface nanoparticles morphologies on the optical band gap and photoluminescence of ZnO thin films deposited by pulsed electron deposition technique. J Mater Sci: Mater Electron 33(9):7236–7243. https://doi.org/10.1007/s10854-022-07906-6

[42] Jumat ZBH, Chou CT, Chou YF, Mahadi AH, Kooh MR, Kumara NT, Chiang HP (2021) Plasmonic refractive index sensor based on the combination of rectangular and circular resonators including baffles. Chin J Phys 71:286–299. https://doi.org/10.1016/j.cjph.2021.02.006

[43] El-Saeed AH, Allam NK (2018) Refractory plasmonics: orientation-dependent plasmonic coupling in TiN and ZrN nanocubes. Phys Chem Chem Phys 20(3):1881–1888. https://doi.org/10.1039/C7CP04933A

[44] Alderman DJ (1985) Malachite green: a review. J Fish Dis 8(3):289–298. https://doi.org/10.1111/j.1365-2761.1985.tb00945.x

[45] Srivastava S, Sinha R, Roy D (2004) Toxicological effects of malachite green. Aquat Toxicol 66(3):319–329. https://doi.org/10.1016/j.aquatox.2003.09.008

[46] He L, Kim N-J, Li H, Hu Z, Lin M (2008) Use of a fractal-like gold nanostructure in surface-enhanced raman spectroscopy for detection of selected food contaminants. J Agric Food Chem 56(21):9843–9847. https://doi.org/10.1021/jf801969v

[47] Song J, Huang Y, Fan Y, Zhao Z, Yu W, Rasco B, Lai K (2016) detection of prohibited fish drugs using silver nanowires as substrate for surface-enhanced Raman scattering. Nanomaterials 6(9):175. https://doi.org/10.3390/nano6090175

[48] Polavarapu L, Porta AL, Novikov SM, Coronado-Puchau M, Liz-Marzán LM (2014) Pen-on-paper approach toward the design of universal surface enhanced Raman scattering substrates. Small 10(15):3065–3071. https://doi.org/10.1002/smll.201400438

[49] Ban R, Yu Y, Zhang M, Yin J, Xu B, Wu D-Y, Wu M, Zhang Z, Tai H, Li J, Kang J (2017) Synergetic SERS enhancement in a metal-like/metal double-shell structure for sensitive and stable application. ACS Appl Mater Interfaces 9(15):13564–13570. https://doi.org/10.1021/acsami.6b15396